THE ROLE OF IMAGING IN OBESITY SPECIAL FEATURE REVIEW ARTICLE

Fat fraction mapping using magnetic resonance imaging: insight into pathophysiology

[1]TIMOTHY JP BRAY, MBBChir, MA, [1]MANIL D CHOUHAN, MBBS, PhD, [1]SHONIT PUNWANI, MBBS, PhD, [2]ALAN BAINBRIDGE, PhD and MARGARET A HALL-CRAGGS, MBBS, MD

[1]Centre for Medical Imaging, University College London, London, UK
[2]Department of Medical Physics, University College London Hospitals, London, UK

Address correspondence to: Prof Margaret A Hall-Craggs
E-mail: *margaret.hall-craggs@nhs.net*

ABSTRACT

Adipose cells have traditionally been viewed as a simple, passive energy storage depot for triglycerides. However, in recent years it has become clear that adipose cells are highly physiologically active and have a multitude of endocrine, metabolic, haematological and immune functions. Changes in the number or size of adipose cells may be directly implicated in disease (*e.g.* in the metabolic syndrome), but may also be linked to other pathological processes such as inflammation, malignant infiltration or infarction. MRI is ideally suited to the quantification of fat, since most of the acquired signal comes from water and fat protons. Fat fraction (FF, the proportion of the acquired signal derived from fat protons) has, therefore, emerged as an objective, image-based biomarker of disease. Methods for FF quantification are becoming increasingly available in both research and clinical settings, but these methods vary depending on the scanner, manufacturer, imaging sequence and reconstruction software being used. Careful selection of the imaging method—and correct interpretation—can improve the accuracy of FF measurements, minimize potential confounding factors and maximize clinical utility. Here, we review methods for fat quantification and their strengths and weaknesses, before considering how they can be tailored to specific applications, particularly in the gastrointestinal and musculoskeletal systems. FF quantification is becoming established as a clinical and research tool, and understanding the underlying principles will be helpful to both imaging scientists and clinicians.

INTRODUCTION

Adipose cells have traditionally been viewed as simple, passive energy storage depots for triglycerides, which release energy in the form of fatty acids through lipolysis during times of metabolic stress. However, in recent years it has become clear that adipose cells are highly dynamic, and have important endocrine, metabolic, haematological, immune and structural functions. For example, adipose cells secrete a wide variety of hormones, growth factors, cytokines, matrix proteins and enzymes which interact with diverse organ systems including the hypothalamo-pituitary axis, pancreas, liver, kidneys, endothelium, skeletal muscle and immune system.[1] Leptin is the most well-known of these factors and has an important role in the regulation of satiety,[2] but a number of other "adipocytokines" also contribute to the regulation of food intake, metabolism, immunity and blood pressure homeostasis.[3] These adipocytokines include adiponectin, which is thought to increase insulin sensitivity,[4] and tumour necrosis factor-α, which is an inflammatory cytokine and may contribute to insulin resistance (IR) and the pro-inflammatory state which is observed in obese patients.[5] Adipose tissue expresses all the components of the renin-angiotensin-aldosterone system, which contributes to the regulation of blood pressure and platelet function,[1] and secretes plasminogen activator inhibitor-1, which is involved in fibrinolysis and is altered in obesity.[1]

Importantly, adipose cells in different locations may have different precursors, cytokine profiles and functions.[1,6] The primary site for adipose cells is in adipose tissue, which consists of subcutaneous adipose tissue, found immediately under the skin, and visceral adipose tissue which surrounds organs such as the liver, bowel, pancreas, kidneys and heart. Additionally, fat can accumulate *within* organs, including the liver, pancreas, heart, muscle and bone marrow; these fat deposits are described as "ectopic fat depots".[7] There is a growing appreciation of the importance of ectopic fat in the pathogenesis of disease;[8–10] *e.g.* hepatic fat is implicated in the pathogenesis of metabolic syndrome, and predicts IR

independent of visceral adipose tissue volume.[10] Similarly, bone marrow adipose tissue has a unique role in the regulation of haematopoiesis, bone turnover and systemic metabolism,[11] and derangements in marrow fat are seen in osteoporosis, obesity, diabetes, metastatic malignancy and haematological disorders. Increased awareness of the importance of these fat depots has led to a demand for noninvasive techniques for measuring organ fat content, in both clinical and research settings.

Proton MRI is ideally suited to fat quantification since the majority of the acquired signal originates from protons in water and fat molecules. Fat and water protons produce signals with slightly different frequencies because their chemical environments give rise to subtle differences in the local magnetic fields they experience; the MR signal, therefore, consists of multiple spectral components which have frequencies separated by a few parts per million (ppm). In a chemical shift-encoded MRI (CSE-MRI) experiment, the interference of these components leads to oscillation in the signal over time, and repeated sampling of the signal at varying echo times (TEs) enables quantification of the fat and water signals.[12] The fat fraction(FF) is defined as the signal arising from fat protons divided by the sum of the signals from fat and water protons. The FF can be used as a quantitative image-based indicator of biological and pathological processes—an imaging biomarker.[13]

Recent years have seen a rapid expansion in the number MR methods available for measuring the FF, each with its own strengths and weaknesses. These methods are being used in clinical trials and in clinical practice,[14–16] but approaches to fat quantification are inconsistent. In clinical practice, simple "in phase and out of phase" imaging is commonly used, but can be misinterpreted and may be inaccurate in the presence of iron or bone.[9,17] In this work, we aimed to highlight the strengths and weaknesses of different MR techniques for fat quantification, and to explain potential confounding factors which may introduce bias into FF measurements. Furthermore, we describe a wide variety of existing and potential applications of FF mapping, including established applications in the liver and more recently introduced applications in bone, muscle and heart. We will argue that, quite apart from its role in passive energy storage, the presence and quantity of fat in a tissue can directly inform us about underlying pathophysiological processes in a wide variety of diseases.
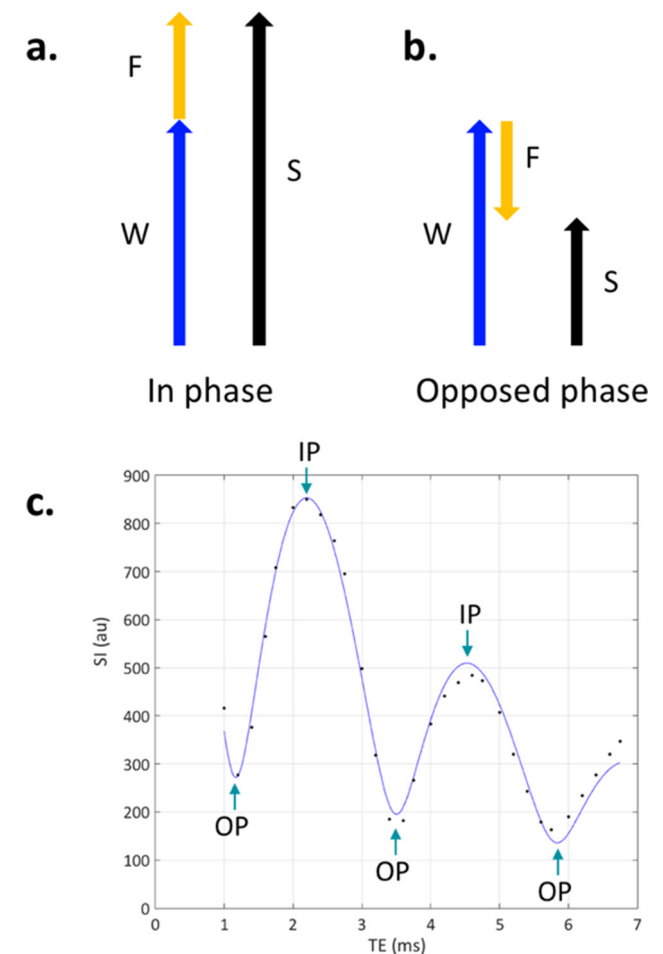
MR METHODS FOR FAT QUANTIFICATION
Dixon's method
The original imaging method for fat quantification ("simple proton spectroscopic imaging") was described by WT Dixon.[12] In Dixon's method, magnitude images were acquired at both "in phase (IP)" and "opposed phase (OP)" TEs, at which times water and fat would constructively and destructively interfere (Figure 1). Water-only and fat-only images (Figure 2) could then be obtained at each voxel by adding and subtracting the two images, respectively.
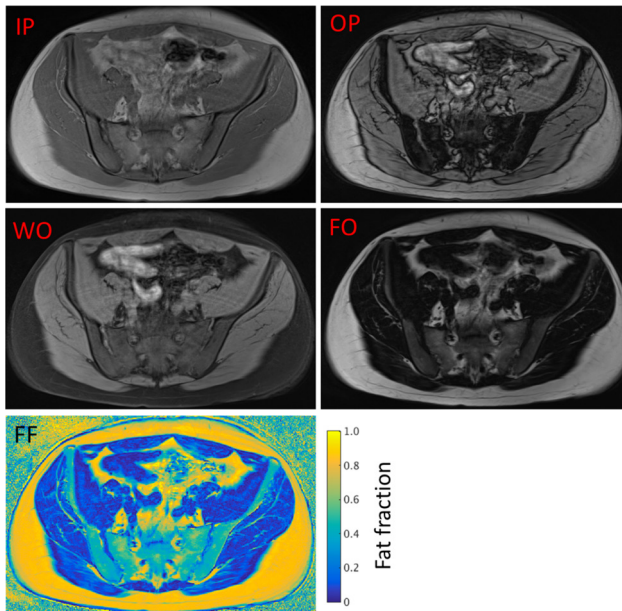
However, Dixon's original method suffered from a major drawback. To overcome problems with background magnetic field

Figure 1. Principles of Dixon imaging. If the image is acquired when the water and fat have the same phase (a), the signals from water (W) and fat (F) constructively interfere, and the total signal $S = W + F$. If the image is acquired when water and fat are in opposed phase (b), W and F destructively interfere and $S = W - F$. (c) Shows data from a single voxel in normal bone marrow (which contains both water and fat), using a gradient echo-based Dixon acquisition with very closely spaced echo times. This data explicitly shows the signal oscillation over time as the fat and water signals dephase, come back into phase,and then dephase again. There is also a progressive reduction in the height of the IP peaks with increasing echo timeowing to signal decay (in this case with the time constant T_2^*).

(B_0) inhomogeneity, Dixon used only magnitude images for the reconstruction (signal phase data were discarded). Any tissue consisting of either pure fat or pure water would, therefore, have approximately equal signal on the IP and OP images. As a result, fatty tissues (such as subcutaneous fat) have high signal on the water images but low signal on the FO images, meaning that the FF measured would be (incorrectly) close to 0%. This phenomenon can potentially cause misinterpretation in clinical practice when in-phase and opposed-phase images are visually compared, since lesions consisting of pure fat exhibit little signal drop-out on opposed images. Furthermore, this is a severe limitation if CSE-MRI is used quantitatively, since

Figure 2. Examples of CSE-MR images. In a two-point CSE-MRI (Dixon) experiment, images are acquired at IP and OP TEs. Addition and subtraction of these images produces water only (WO) and fat only (FO) images, respectively. Fat fraction (FF) maps can then be generated from the WO and FO images as described above.

measured FF values will be inaccurate or heavily biased by fat-water ambiguity.

Extended two-point methods

To overcome the fat-water ambiguity problem, several authors extended Dixon's method to enable resolution of the ambiguity between water-dominant and fat-dominant tissues.[18,19] These extended methods involve the acquisition of complex-valued images (*i.e.* images with both magnitude and phase data) at in phase and out of phase echo times; the phase data is used to distinguish between fat-dominant and water-dominant tissues.

Although these extended two-point methods are a substantial advance on Dixon's original method, they are somewhat susceptible to the effects of B_0 inhomogeneity, since it can be difficult to differentiate between phase shifts owing to B_0 effects and phase shifts due to chemical shift. One approach to reducing the effect of B_0 inhomogeneity is to combine these two-point methods with phase-unwrapping or region-growing algorithms (fat-water separation is usually straightforward if the phase can be successfully unwrapped).[18,19] Unfortunately, these algorithms are somewhat complex and tend to fail in areas of signal cancellation, particularly where the fat and water signals have similar magnitude.

Three-point methods

To eliminate the need for complex region-growing methods and to improve estimation of B_0 inhomogeneity, Glover and Schneider introduced a three-point CSE-MRI method enabling direct estimation of field inhomogeneity to remove its effects from the signal.[20] In this method, one IP echo and two OP

echoes are used; any phase shift between the two opposed phase echoes can be attributed to B_0 inhomogeneity, which can be used to correct the acquired signals. Glover and Schneider's method was subsequently extended to allow greater flexibility with regard to echo times by Xiang and An[21], and a three-point method using a similar approach has recently been introduced for whole body imaging.[22] These three-point methods form the basis of a number of manufacturers' methods for rapid fat-suppressed imaging, primarily due to their speed and relative robustness to artifacts.[23,24] However, where FFs need to be calculatedly accurately, a different approach is necessary.

Maximum -likelihood estimation

The extended two-point and three-point methods described above were only intended to separate two species (water and fat). In practice, the two-species assumption leads to inaccuracies in fat quantification, since human fat actually consists of a number of spectral fat components (the "main" fat peak comes from hydrogen atoms in methylene residues, but methyl, allylic and olefinic residues also contribute substantially to the measured signal).[25] Furthermore, these methods do not account for T_2^* decay, which can introduce a further source of bias.[25,26]

To account for the effects of spectral fat complexity and T_2^* decay and thereby reduce bias, a maximum-likelihood method can be used to find the parameters in a pre-specified signal model which will most closely fit the acquired data.[27] This approach was first proposed by Xiang and An, who used a non-linear least squares (NLLS) method with a signal model assuming multiple spectral fat components. Subsequently, a more general maximum-likelihood method—echo asymmetry and least squares estimation [IDEAL (iterative decomposition of water and fat with echo asymmetry and least squares estimation)]—was proposed and developed by Reeder et al[28,29] The IDEAL method enables an arbitrary choice of echo times (and, importantly, can be easily applied to acquisitions with more than three echoes) and arbitrary numbers of spectral components. IDEAL can also be adapted to account for T_2^* decay, which substantially improves the accuracy of fat quantification in the presence of liver, and has been shown to be an accurate measure of fat content both in phantoms and in patients with hepatic steatosis.[9,25] IDEAL has formed the basis of a number of commercially available algorithms for fat quantification designed for liver imaging, and has been widely used in medical imaging research.[30–33]

Nonetheless, IDEAL also has limitations. The critical step in the IDEAL algorithm is the estimation of the B_0 field map; however, this always involves a degree of ambiguity, and an incorrect B_0 estimation may occur in areas of large inhomogeneity. Modifications to the IDEAL method using region-growing or graph-cut methods can be used to improve performance in the presence of B_0 inhomogeneity,[34,35] but fat-water swaps remain difficult to prevent entirely, and algorithm development remains an area of active research.

MR spectroscopy

The "gold standard" modality for fat quantification is magnetic resonance spectroscopy (MRS), which typically uses point-

resolved spectroscopy or stimulated echo acquisition mode single-voxel sequences.[9,33,36] Spectra can be used to determine both the fat fraction and the specific composition of the fat, including fatty acid composition parameters. However, MRS cannot be used to generate FF maps, and CSE-MRI methods, which allow for high-resolution imaging, are therefore more attractive for medical applications. This is particularly important in the measurement of organ fat where distribution may be spatially heterogenous.

The fat fraction as a biomarker: properties and confounders

Two characteristics of primary importance when measuring FF are accuracy and precision.[37] Accuracy can be viewed as the correctness of a biomarker measurement in comparison to a reference standard (an accurate biomarker demonstrates low bias and high linearity), whilst precision is a measure of measurement consistency.[13,37] The accuracy of FF measurements can be determined using fat-water phantoms, typically consisting of emulsions of fat and water which are solidified using agar or thickened using carrageenan.[25,38] Measured FF values can then be directly compared with known fat fraction values in the phantom. Precision (repeatability and reproducibility) of measurements is typically determined using repeat scans, often across multiple scanners and sites.[39]

Depending on the acquisition, FF measurements may be biased by T_1 and $T_2/T_2^\star$ relaxation, the presence of multiple fat peaks noise, phase errors, B_1-inhomogeneity and J-coupling.[13] The bias may be minimized by optimizing acquisition parameters, and/or by using post-processing correction strategies.

T_1-bias can be minimized by using a low flip angle (typically 5° or less) and long repetition times. For gradient echo acquisitions, an important consideration is the number of echoes acquired, since later echoes are subject to a longer period of $T_2^\star$ decay.[40] Using maximum-likelihood estimation, $T_2^\star$ decay can be incorporated into signal models and, therefore, corrected for—this is particularly important in organs containing significant quantities of iron or mineralized bone where $T_2^\star$ will be short.[26,41] To minimize the effect of the spectral complexity of fat, a predefined fat spectrum can be assumed. All CSE-MRI algorithms are also dependent on the choice of echo time, echo spacing and the presence of noise.[42]

If all potential sources of bias are eliminated, the FF can then be described as a proton density fat fraction (PDFF)—this is the ratio of unconfounded fat signal to the sum of the unconfounded fat and water signals.[43] FF measurements which are still biased by one or more of these factors may be referred to as signal FFs (sFF). Accurate measurement of PDFF potentially enables comparison of values between scanners, and across multiple sites. Data from multisite, multivendor studies suggest that the reproducibility of "confounder-corrected" PDFF measurements is excellent in the liver,[39,44] although further work is required to examine reproducibility for other applications. Reproducibility is a major strength of CSE-MRI and makes this technique attractive for use in research and clinical practice.

Practical implementation: choosing a technique

Deciding on an imaging acquisition and post-processing method for FF mapping can be a somewhat bewildering process, owing to the large variety of acquisition and post-processing methods available. The most important choice is whether to use a manufacturer-implemented solution, with inline processing on the scanner, or to acquire raw data for offline processing. On most modern scanners, users should have access to simple two- or three-point methods. The major manufacturers also offer dedicated packages for PDFF measurement, which measure and correct for $T_2^\star$ decay and other confounds, and produce PDFF maps inline. The major advantage of this approach is ease of use; the disadvantage is that the details of the processing methodology are generally not available to the user. Conversely, acquiring raw magnitude and phase images enables offline processing using a chosen reconstruction method, but is dependent on the availability of local expertize and may not be feasible for some centres. However, a number of commonly used methods for post-processing, including analytical three-point methods, versions of the IDEAL algorithm and graph cut-based methods, are available through the International Society of Magnetic Resonance in Medicine fat-water toolbox.[13] This toolbox enables the user to try different algorithms on their own datasets, enabling them to find a method which works well with their data and suits their specific requirements. At our institution UCLH/UCL), we typically use a 3D multiecho gradient echo acquisition from which we are able to reconstruct both PDFF and $R_2^\star$ maps using the manufacturer PDFF product, and also extract raw magnitude and phase images for offline-reconstruction. Typical acquisition parameters for manufacturer-implemented sequences for PDFF measurement are given in Table 1; similar parameters can also be used if raw complex data is acquired. For abdominal applications, these parameters allow for good anatomical coverage with a scan time short enough for acquisition within a breath-hold.

How many points?

The ideal situation is to use an acquisition which allows for true PDFF measurement, which generally involves acquiring more than three echoes (at our institution we use six). However, depending on the clinical problem, meaningful FF measurements may be obtained using simple two- or three-point methods. For example, patients with haematological malignancies undergo relatively large changes in FF compared to normal marrow (and with treatment) and a simple sFF measurement is sufficient to demonstrate a clinically meaningful effect.[45] Conversely, in patients with hepatic steatosis, relatively small variations in FF can be clinically relevant, whilst $T_2^\star$ effects can cause a significant bias—a true PDFF measurement is, therefore, required.[9] The choice of acquisition, therefore, depends on the range of values expected in normal tissue, the size of the change expected in disease and the post-processing software which is available to the user.

Echo times

When setting up a CSE-MRI acquisition, the first echo time (TE_1) and echo spacing (ΔTE) need to be optimized. In general, using a shorter ΔTE reduces the sensitivity of the technique to

Table 1. Typical imaging parameters for liver PDFF imaging using manufacturer-implemented PDFF products

Parameter	Philips	Siemens	GE
PDFF manufacturer-supplied package	mDixon Quant	DIXON FQ in Liver Lab package	IDEAL IQ
Sequence variant	3D spoiled gradient echo	3D spoiled gradient echo	3D spoiled gradient echo
Imaging time	Breath-hold (<20 s)	Breath-hold (< 20 s)	Breath-hold (< 20 s)
TR	Shortest (5–10ms)	Shortest (5–10ms)	Shortest (5–10ms)
Number of echoes	6	6	6
TE of first echo (TE_1)	Shortest (~0.8–1.5ms)	Shortest (~ 0.8–1.5ms)	Shortest (~ 0.8–1.5ms)
Echo spacing (ΔTE)	Shortest (~0.8–1.5ms)	Shortest (~ 0.8–1.5ms)	Shortest (~ 0.8–1.5ms)
Flip angle	3°	3°	3°
Parallel imaging factor	2	2	2
Number of averages	1	1	0.5
Number of shots	–	–	2
Reconstructed images	Fat-only image Water-only image PDFF map T_2* map	Fat-only image Water-only image PDFF map T_2* map	Fat-only image Water-only image PDFF map T_2* map

IDEAL, iterative decomposition of water and fat with echo asymmetry and least squares estimation; PDFF, proton density fat fraction; TE, echo time; TR, repetition time.

B_0 inhomogeneity (effectively increasing the spectral resolution), thereby improving the quality of fat-water decomposition.[13] However, a balance needs to be struck between image resolution (higher resolution necessitates longer readouts, and therefore larger ΔTE), and fat-water decomposition quality. At our institution, we typically use a multiecho acquisition with TE_1 of 0.5–1.5 ms and ΔTE 0.8–1.5 ms.

Applications
Hepatic steatosis and the metabolic syndrome
Metabolic syndrome (MetS) is a group of risk factors for cardiovascular disease, diabetes and stroke, which includes obesity, dyslipidaemia, hypertension and raised fasting blood glucose.[46] Although current definitions of MetS do not include hepatic steatosis, the association between liver fat and MetS is becoming increasingly clear.[47–49] Furthermore, non-alcoholic fatty liver disease (NAFLD) is the most common cause of chronic liver disease in the Western world.[50] As such, there is a clinical need for simple, non-invasive tools for measuring liver fat. Hepatic steatosis (increased liver fat content) was one of the earliest applications of the Dixon method, and remains one of the most important.

Hepatic steatosis may be either primary (in the case of NAFLD), or secondary, *e.g.* owing to alcoholic liver disease, drug-toxicity, hepatitis, pregnancy and parenteral nutrition. NAFLD is defined by the presence of hepatic steatosis in the absence of any secondary cause, and lies on the benign end of a spectrum with non-alcoholic steatohepatitis (NASH), which is a more aggressive disease entity associated with cirrhosis, hepatocellular carcinoma and end-stage liver disease.

Underpinning MetS is the phenomenon of insulin resistance (IR), whereby increasing insulin levels are required to achieve a normal metabolic response, or normal insulin levels fail to provide a normal metabolic response.[51] Accumulation of fat within hepatocytes is driven by IR through increases in peripheral lipolysis and *de novo* lipogenesis, and through reductions in beta-oxidation of fatty acids within hepatocytes.[52,53] Accumulation of intracellular lipid within hepatocytes is the first part of the "two-hit" hypothesis,[54] after which increased vulnerability to oxidative stress, lipid peroxidation, inflammation and mitochondrial dysfunction in combination cause chronic hepatocyte injury, fibrosis and NASH.[55] The widespread prevalence of NAFLD has thus become a major healthcare focus, not only to try to avoid the much more aggressive NASH phenotype which may evolve if untreated, but also as a potential therapeutic target to address cardiovascular disease and diabetes mellitus.

The diagnosis of steatosis can be made histologically, but both the European Association for the Study of the Liver[56] and the American Association for the Study of Liver Disease[57] use MRI-based criteria to define the condition. For example, the EASL guidelines use a threshold of > 5% as measured using PDFF, or > 5.6% by MRS. MRS has been seen as the non-invasive gold-standard for quantitative assessment of liver fat,[8] but the technical complexity associated with MRS acquisitions and the spatial heterogeneity of hepatic steatosis have led to the widespread use of imaging-based methods for assessment of steatosis.[58]

Numerous studies have now demonstrated the accuracy of PDFF measurements using CSE-MRI as compared with MRS,[8,59] histology[60–62] or both,[24,60,63–65] and the reproducibility of PDFF measurements is excellent—Hernando et al[39] found an overall intraclass correlation coefficient of 0.999 on repeat scans across sites, field strengths and vendors (example of PDFF of normal liver and NAFLD shown in Figure 3). Similarly, a large meta-analysis including data from > 1000 patients has demonstrated 95%

Bland-Altman limits-of-agreement of ± 4% for liver PDFF *vs* MRS, with liver PDFF reproducibility coefficients of 4.3% across different scanner vendors.[66] PDFF measurements are strongly correlated with quantitative histopathological assessment of liver fat.[61,63,67,68] Furthermore, longitudinal studies have suggested that PDFF may be more sensitive than histological quantification for early steatosis.[69,70]

The data from these validation studies have supported the use of liver PDFF measurements in clinical trials. PDFF measurements have recently been used as endpoints in double-blind randomized, placebo-controlled trials of colesevelam and ezetimibe for NASH,[14,69] and of insulin glargine and liraglutide for poorly controlled Type2 diabetes.[71] These studies highlight the value of PDFF measurements as primary outcome measures for high quality randomized controlled trials evaluating the next generation of treatments for NASH, NAFLD and diabetes.

With a progressively established role for liver PDFF measurements in the research setting, there are several challenges facing routine clinical implementation. Hepatic steatosis is a spatially heterogeneous process,[72] and there is some debate about how to condense the information stored in imaging maps into simple indices that can be used by clinicians.[71,73,74] Quantitative liver imaging remains in its infancy, but PDFF has a justified role alongside other quantitative methods (such as T_1 mapping) in multiparametric MRI.[75] One of the major advantages of PDFF acquisitions is that T_2^* maps, which have a role in the quantification of liver iron, can be generated simultaneously. This means that two quantitative parametric maps reflecting different aspects of liver physiology can be generated quickly and simply.

Pancreatic fat – the missing link?

Qualitative assessment of pancreatic fat accumulation is readily undertaken using anatomical MRI, but it can be difficult to separate "fatty infiltration" from small volume "fatty replacement" as these can often occur simultaneously.[76] Structural im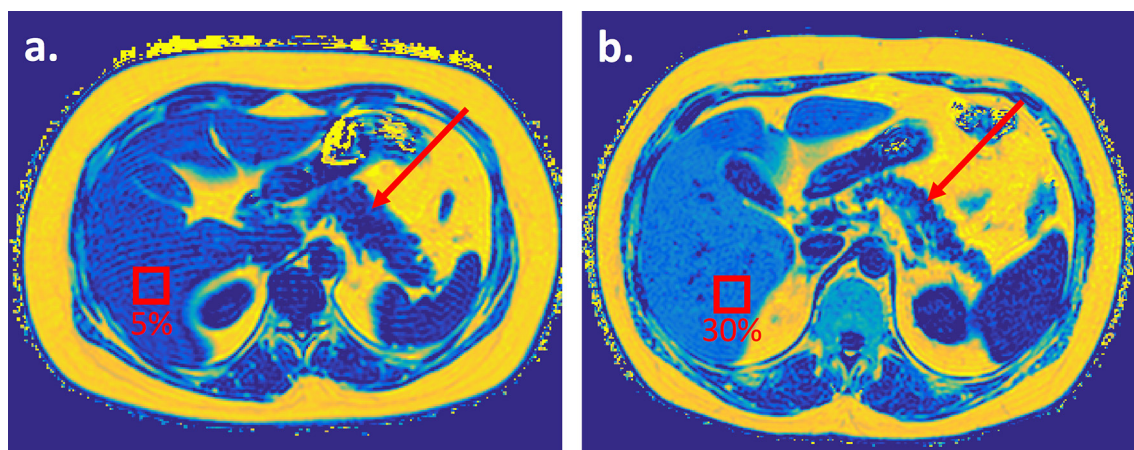aging changes in pancreatic steatosis include accumulation of extra-, inter- and intralobular fat, in addition to intracellular accumulation of fat, yet the clinical significance of each of these processes remains unknown. As a result, some groups have recently begun to use quantitative MRI to investigate the role of pancreatic fat.

Pancreatic steatosis research has been hampered by confusing nomenclature (*e.g.* pancreatic lipomatosis, fatty pancreas, fatty infiltration), but the more recent label of non-alcoholic fatty pancreas disease is gradually gaining acceptance.[77] Non-alcoholic fatty pancreas disease can occur secondary to several causes (age, viral infections including HBV and HIV, drug-related causes, haemochromatosis and congenital causes), but it is the association with metabolic causes (obesity and diabetes mellitus) that has driven interest in this area of research.[78]

Histologically, pancreatic steatosis is a heterogeneous process characterized by increased intracellular lipid accumulation followed by rising pancreatic adipocytes within pancreatic tissue.[79] A recent meta-analysis quantified normal mean pancreatic fat at 4.5 ± 0.9% (based on pooled data across multiple MR methods and imaging modalities),[80] but precise consensus thresholds have yet to be defined. It is possible that triglyceride overload may contribute to beta-cell dysfunction in Type 2 diabetes, although a causal relationship between pancreatic steatosis and diabetes remains unproven.[81] Current evidence regarding the relationship between pancreatic fat, body mass index, diabetes, MetS and IR is somewhat conflicting and the nature of these links remains unclear.[82,83] Some large-scale studies have demonstrated relationships with IR,[84,85] but others have failed to find a consistent link between age, body mass index, incidence of Type 2 diabetes.[84,86,87]

Histological validation studies suggest reasonable agreement between histological measures and PDFF, although the repeatability of the measurement is arguably suboptimal (Yoon et al[88] found Bland-Altman 95% limits of agreement of ± 17% for pancreatic PDFF measurement). There are several specific

Figure 3. PDFF maps of a comparable axial slice through the abdomen in two subjects. Despite having comparable subcutaneous and intraperitoneal fat volumes, there is differing intravisceral fat with (a) low hepatic and pancreatic fat and (b) NAFLD, with heterogeneous left and right steatosis and pancreatic interlobular fatty infiltration. The pancreas is arrowed on both subjects, and regions of interest have been placed on the liver to demonstrate differences in hepatic PDFF.

methodological issues which may contribute to problems with repeatability in the pancreas, including the presence of motion artefact, differences in the composition of fat compared to liver and the fact that pancreatic fat is separated into extra-, inter- and intralobular compartments. Just as in the liver, $T_2{}^*$ decay needs to be accounted for (and may also be a useful biomarker in its own right), particularly in iron-deposition disorders such as haemochromatosis.[89,90]

Osteoporosis, obesity and the fat-bone connection

Osteoporosis and obesity are increasingly important public health problems, and are associated with a large burden of morbidity and mortality. Although these diseases are seemingly disparate, both can be traced to the dysfunction of a common progenitor cell—the bone marrow mesenchymal stem cell (MSC). MSCs can differentiate into either adipocytes or osteoblasts depending on their cytokine environment and stromal interactions.[91] Furthermore, adipocytes themselves (which express a variety of paracrine and endocrine factors) may actively influence MSC differentiation and, therefore, affect bone remodeling.[91]

Multiple studies have demonstrated an inverse relationship between marrow fat content and bone mineral density or bone formation rate,[92–95] such that osteoblast activity and bone formation rates are both decreased at sites of high marrow fat.[96,97] This has led to a the suggestion that osteoporosis is the "obesity of bone".[91] Several animal studies have indicated that adipose cells may directly reduce bone mass through the action of leptin.[98,99] However, the precise role of marrow fat in the regulation of bone formation in humans remains unclear, and changes in marrow fat content may partly reflect a passive response to bone loss.[11,91,100,101] It may be that changes in marrow fat contribute to the pathogenesis of certain subtypes of osteoporosis, but not others.[11]

In patients with obesity *per se*, both visceral and bone marrow fat are again adversely associated with bone microarchitecture.[102] Visceral fat may negatively impact on bone health via modifying insulin-like growth factor-1 (IGF-1) levels; vertebral bone marrow fat in postmenopausal females is negatively associated with BMD and IGF-1, but positively associated with visceral fat.[103] Since bone and fat cells have the same mesenchymal precursor, IGF-1 may influence BMD through its effect on MSC differentiation (into fat or bone lineages).[103] Accordingly, mice with IGF-1 suppression have fatty infiltration of the marrow and liver and markedly reduced BMD, although they are not obese.[104]

Impairments in bone microarchitecture are also observed in diabetic patients, who have an increased fracture risk.[105] Again, this may occur because obesity and IR cause osteoblast and osteoclast dysfunction and, therefore, reduced bone turnover.[105,106] Studies of patients with Type2 diabetes have not revealed significant differences in marrow FF compared to controls, although multiple studies have found that diabetic patients have a greater proportion of unsaturated fat.[107,108] Conversely, the proportion of unsaturated fat in the marrow is thought to decrease in osteoporosis, although the significance of this finding is unclear.[109]
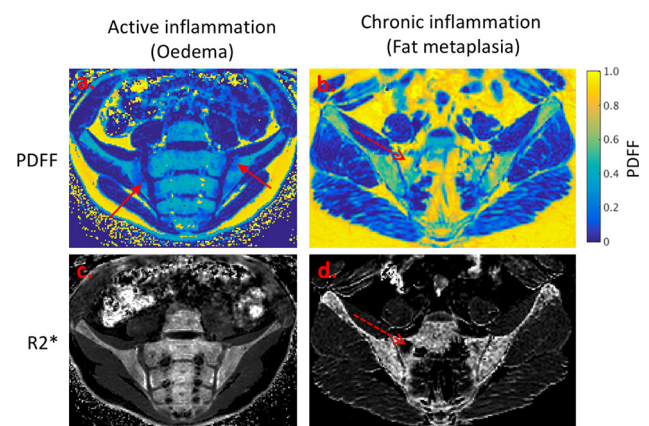
Paradoxically, bone marrow fat is increased in anorexia nervosa despite losses in overall body fat.[110,111] A possible explanation is that marrow adipose tissue increases represent a homeostatic response designed to increase appetite and promote insulin sensitivity;[11] alternatively, marrow adipose tissue may be maintained in spite of overall adipose tissue loss owing to its role in haematopoiesis and bone turnover.[11]

FF as a marker of malignant infiltration in bone

In multiple myeloma (MM), the rapid development of novel therapeutic strategies requires improved disease staging techniques. Whole-body MRI (WB-MRI) is now widely available, relatively cheap and establishing itself as a first-line imaging modality in MM.[112,113] CSE-MRI may be used as a fast "anatomical" imaging modality and enables the simultaneous generation of up to four image types using a single sequence (in phase, out of phase, WO and FO), which are used for qualitative interpretation. Additionally, quantitative FF measurements may be used as a marker of marrow composition, and are thought to reflect the proportion of haematopoietic (red) and fatty (yellow) marrow, which may be altered by malignant infiltration.[114] Patients with symptomatic MM have significantly lower PDFF measurements than those with asymptomatic disease.[114] Furthermore, recent work analysing sFF measurements in focal MM lesions suggests that sFF measurements may stratify patients according to their depth of therapeutic response.[45] sFF measurements appear to be better discriminator of response than alternative tumour volume or apparent diffusion coefficient (ADC) values.[45]

CSE-MRI may also be used to detect skeletal metastases in patients with solid tumours, and is reasonably sensitive and specific (70.8 and 89.1%, respectively).[115] FF measurements are also reduced in patients with a malignancy but without skeletal involvement, possibly reflecting red marrow proliferation FF owing to systemic effects of malignancy or drugs.[116]

Figure 4. Emerging application of PDFF and $R_2{}^*$ measurement in spondyloarthritis. Areas of active inflammation (a, c) demonstrate a reduction in fat content, but no change in $R_2{}^*$. Areas of chronic inflammation (fat metaplasia) (b, d) demonstrate an increase in fat content, and a reduction in $R_2{}^*$ which may indicate local osteoporosis.

FF as a measure of skeletal inflammation

An emerging application for PDFF measurements is in patients with spondyloarthritis (SpA), in whom quantification of inflammation is important for guiding disease-modifiying and biological therapy.

MRI is commonly used to diagnose and monitor axial inflammation in SpA,[117] but current clinical imaging protocols consist mostly of conventional T_1 weighted, T_2 weighted and short tau inversion recovery spin echo sequences, which can be subjectively interpreted by a radiologist to give a semi-quantitative inflammatory "score".[118] However, visual scoring of inflammation suffers from relatively poor reproducibility - Arnak et al[119] reported kappa coefficients of 0.85 for the presence of bone marrow oedema, and 0.61 for global diagnosis of SpA using MRI- and is, therefore, not widely used in clinical practice. PDFF measurements have, therefore, been investigated as an objective tool for quantifying active inflammation (*i.e.* bone marrow oedema) and chronic inflammation (which causes an increase in marrow fat content known as fat metaplasia) ([Figure 4]).[120] PDFF measurements are reduced in areas of active inflammation (likely owing to an increase in water content caused by the inflammatory exudate), but increased in areas of chronic inflammation, possibly owing to the effect of inflammatory cytokines on MSC differentiation.[120] FF measurements in bone marrow are accurate in fat-water phantoms and have been found to offer excellent reproducibility (reported intraclass correlation coefficient values for PDFF in bone vary from 0.87 to 0.98).[120, 121] They may, therefore, provide a more reliable measurement of inflammatory severity than visual interpretation. A further advantage is that simultaneously generated R_2^* (*i.e.* $1/T_2^*$) maps are thought to report on BMD, and may provide a measure of new bone formation and bone destruction (both of which are key processes in SpA).[120]

FF in neuromuscular diseases

Neuromuscular diseases involve a range of pathological processes including inflammation, muscle atrophy and fat infiltration, all of which may contribute to functional disability. The lack of sensitive, responsive outcome measures has been a barrier to the development of novel therapies for neuromuscular diseases, and there has, therefore, been a drive to develop imaging markers of disease activity and muscle damage.

Morrow et al[122] showed that whole muscle FF measurements were altered in patients with both Charcot-Marie-Tooth disease and inclusion body myositis, highly responsive to change and correlated with conventional functional measures.[122] Different imaging biomarkers appear to reflect different disease processes—Yao et al[123] showed that muscle T_2 and fat-corrected T_2 measurements were correlated with visual inflammation scores, whilst FF measurements correlated with damage scores, in patients with idiopathic inflammatory myopathy. Technical developments in CSE-MRI methods may enable simultaneous quantitation of inflammation and damage. Recently, Janiczek et al[31] described a technique for simultaneous quantitation of T_2 of water, T_2 of fat and fat fraction in a patient with inclusion body myositis, which revealed disease-specific

patterns of fat infiltration and oedema. Similarly, in patients with myotonic dystrophy, Hiba et al demonstrated a clear relationship between disease severity and FF measurements in the tibialis anterior.[124] There is preliminary evidence that subclinical progression may be reflected by changes in FF.[122] FF measurements also agree closely with histological measures of fat infiltration.[125] Given the increases in fat content which invariably accompany muscle damage, FF measurements are likely to have an increasingly important role in therapeutic trials and, ultimately, in the clinic.

Cardiac and vascular applications of CSE-MRI

Intramyocardial fat may arise in both ischaemic and nonischaemic cardiomyopathies, and is associated with a poor prognosis.[126] So-called "lipomatous metaplasia" is common in ventricular scar tissue following myocardial infarction,[127–129] and the transformation of compact scar into compressible "sliding" adipose tissue may worsen ventricular function, frequently resulting in severe heart failure.[129] In patients with dilated cardiomyopathy, fat deposition is associated with increased end-diastolic and end-systolic volumes, decreased left ventricular ejection fraction and increased late gadolinium enhancement (a marker of fibrosis).[130] A causal link between myocardial fat and functional impairment is currently unproven, although accumulated fat (either within adipocytes or the myocytes themselves) may be directly toxic to the myocardium. It has been suggested that lipid accumulation may sometimes be a precursor to myocardial infarction, potentially due to metabolic changes resulting from low-grade ischaemia, although this suggestion remains unproven.[131]

Cardiac fat quantification studies have relied on multiecho Dixon-like methods, which are sensitive to small concentrations of myocardial fat.[28–35] These methods are typically ECG-gated, which enables acquisition of data during diastole and a subsequent improvement in resolution compared to non-gated methods.[132] Although "conventional" fat suppression using chemical shift selective pulses can also be used in the heart, Dixon-like methods offer superior fat-water decomposition in the presence of B_0 inhomogeneity.[132] Similar to imaging other organs, T_1 and T_2^* decay and noise can potentially confound FF measurements, but can be corrected for.[133] Once this correction has been performed, PDFF measurements using Dixon MRI agree closely with MRS measurements.[133]

Finally, FF and R_2^* measurements may be valuable as markers of plaque composition in patients with carotid atherosclerosis – Koppal et al[41] showed that FF measurements reflect lipid composition, whilst R_2^* measurements reflect intraplaque haemorrhage.

PERSPECTIVES AND CONCLUSION

Far from being an inert energy store, adipose cells are highly physiologically active and have an extensive role in both normal physiology and disease. CSE-MRI is rapidly emerging as the primary clinical and research tool for fat quantification, and has a multitude of existing and emerging applications. Although abdominal fat quantification in obesity and metabolic syndromes are among the most obvious, there are a multitude of

applications for CSE-MRI in the muscle, bone, heart and vessel wall.

Nonetheless, there are several barriers to the widespread use of CSE-MRI in clinical practice. Although most manufacturers now offer CSE-MRI packages, the bewildering array of options, confusing nomenclature and overall cost can discourage radiology departments from using these methods. Technical problems with transferring FF maps on to picture archiving and communication system software may also reduce the practicality of using CSE-MRI. However, as awareness and availability of CSE-MRI increase, these issues are likely to resolve. Novel post-processing technologies such as organ segmentation and machine learning may also help the radiologist to maximize the information which can be extracted from FF maps. Looking forward, we anticipate that FF mapping will become a mainstay of clinical radiology, and will be used to objectively characterize disease in a wide variety of organ systems. The FF is here to stay.

FUNDING

REFERENCES

1. Coelho M, Oliveira T, Fernandes R. Biochemistry of adipose tissue: an endocrine organ. *Arch Med Sci* 2013; **9**: 191–200. doi: https://doi.org/10.5114/aoms.2013.33181

2. Zhang Y, Proenca R, Maffei M, Barone M, Leopold L, Friedman JM. Positional cloning of the mouse obese gene and its human homologue. *Nature* 1994; **372**: 425–32. doi: https://doi.org/10.1038/372425a0

3. Matsuzawa Y. The metabolic syndrome and adipocytokines. *FEBS Lett* 2006; **580**: 2917–21. doi: https://doi.org/10.1016/j.febslet.2006.04.028

4. Stępień M, Wlazeł RN, Paradowski M, Banach M, Rysz M, Misztal M, et al. Serum concentrations of adiponectin, leptin, resistin, ghrelin and insulin and their association with obesity indices in obese normo- and hypertensive patients - pilot study. *Arch Med Sci* 2012; **8**: 431–6. doi: https://doi.org/10.5114/aoms.2012.29397

5. Cai D, Yuan M, Frantz DF, Melendez PA, Hansen L, Lee J, et al. Local and systemic insulin resistance resulting from hepatic activation of IKK-β and NF-κB. *Nat Med* 2005; **11**: 183–90. doi: https://doi.org/10.1038/nm1166

6. Sethi JK, Vidal-Puig AJ. Thematic review series: adipocyte biology. Adipose tissue function and plasticity orchestrate nutritional adaptation. *J Lipid Res* 2007; **48**: 1253–62. doi: https://doi.org/10.1194/jlr.R700005-JLR200

7. Thomas EL, Fitzpatrick JA, Malik SJ, Taylor-Robinson SD, Bell JD. Whole body fat: content and distribution. *Prog Nucl Magn Reson Spectrosc* 2013; **73**: 56–80. doi: https://doi.org/10.1016/j.pnmrs.2013.04.001

8. Reeder SB, Cruite I, Hamilton G, Sirlin CB. Quantitative assessment of liver fat with magnetic resonance imaging and spectroscopy. *J Magn Reson Imaging* 2011; **34**: 729–49. doi: https://doi.org/10.1002/jmri.22580

9. Meisamy S, Hines CD, Hamilton G, Sirlin CB, McKenzie CA, Yu H, et al. Quantification of hepatic steatosis with T1-independent, T2-corrected MR imaging with spectral modeling of fat: blinded comparison with MR spectroscopy. *Radiology* 2011; **258**: 767–75. doi: https://doi.org/10.1148/radiol.10100708

10. Müller MJ, Lagerpusch M, Enderle J, Schautz B, Heller M, Bosy-Westphal A. Beyond the body mass index: tracking body composition in the pathogenesis of obesity and the metabolic syndrome. *Obes Rev* 2012; **13** (Suppl 2): 6–13. doi: https://doi.org/10.1111/j.1467-789X.2012.01033.x

11. Scheller EL, Rosen CJ. What's the matter with MAT? Marrow adipose tissue, metabolism, and skeletal health. *Ann N Y Acad Sci* 2014; **1311**: 14–30. doi: https://doi.org/10.1111/nyas.12327

12. Dixon WT. Simple proton spectroscopic imaging. *Radiology* 1984; **153**: 189–94. doi: https://doi.org/10.1148/radiology.153.1.6089263

13. Hu HH, Börnert P, Hernando D, Kellman P, Ma J, Reeder S, et al. ISMRM workshop on fat-water separation: insights, applications and progress in MRI. *Magn Reson Med* 2012; **68**: 378–88. doi: https://doi.org/10.1002/mrm.24369

14. Loomba R, Sirlin CB, Ang B, Bettencourt R, Jain R, Salotti J, et al.Ezetimibe for the treatment of nonalcoholic steatohepatitis: assessment by novel magnetic resonance imaging and magnetic resonance elastography in a randomized trial (MOZART trial). *Hepatology* 2015; **61**: 1239–50. doi: https://doi.org/10.1002/hep.27647

15. Patel NS, Doycheva I, Peterson MR, Hooker J, Kisselva T, Schnabl B, et al. Effect of weight loss on magnetic resonance imaging estimation of liver fat and volume in patients with nonalcoholic steatohepatitis. *Clin Gastroenterol Hepatol* 2015; **13**: 561–8. doi: https://doi.org/10.1016/j.cgh.2014.08.039

16. Andersen G, Dahlqvist JR, Vissing CR, Heje K, Thomsen C, Vissing J. MRI as outcome measure in facioscapulohumeral muscular dystrophy: 1-year follow-up of 45 patients. *J Neurol* 2017; **264**: 438–47. doi: https://doi.org/10.1007/s00415-016-8361-3

17. Gee CS, Nguyen JT, Marquez CJ, Heunis J, Lai A, Wyatt C, et al. Validation of bone marrow fat quantification in the presence of trabecular bone using MRI. *J Magn Reson Imaging* 2015; **42**: 539–44. doi: https://doi.org/10.1002/jmri.24795

18. Coombs BD, Szumowski J, Coshow W. Two-point Dixon technique for water-fat signal decomposition with B0 inhomogeneity correction. *Magn Reson Med* 1997; **38**: 884–9. doi: https://doi.org/10.1002/mrm.1910380606

19. Skinner TE, Glover GH. An extended two-point Dixon algorithm for calculating separate water, fat, and B0 images. *Magn Reson Med* 1997; **37**: 628–30. doi: https://doi.org/10.1002/mrm.1910370426

20. Glover GH, Schneider E. Three-point Dixon technique for true water/fat decomposition with B0 inhomogeneity correction. *Magn Reson Med* 1991; **18**: 371–83. doi: https://doi.org/10.1002/mrm.1910180211

21. Xiang QS, An L. Water-fat imaging with direct phase encoding. *J Magn Reson*

Imaging 1997; **7**: 1002–15. doi: https://doi.org/10.1002/jmri.1880070612

22. Berglund J, Johansson L, Ahlström H, Kullberg J. Three-point Dixon method enables whole-body water and fat imaging of obese subjects. *Magn Reson Med* 2010; **63**: 1659–68. doi: https://doi.org/10.1002/mrm.22385

23. Eggers H, Brendel B, Duijndam A, Herigault G. Dual-echo Dixon imaging with flexible choice of echo times. *Magn Reson Med* 2011; **65**: 96–107. doi: https://doi.org/10.1002/mrm.22578

24. Kukuk GM, Hittatiya K, Sprinkart AM, Eggers H, Gieseke J, Block W, et al. Comparison between modified Dixon MRI techniques, MR spectroscopic relaxometry, and different histologic quantification methods in the assessment of hepatic steatosis. *Eur Radiol* 2015; **25**: 2869–79. doi: https://doi.org/10.1007/s00330-015-3703-6

25. Hines CD, Yu H, Shimakawa A, McKenzie CA, Brittain JH, Reeder SB. T1 independent, T2* corrected MRI with accurate spectral modeling for quantification of fat: validation in a fat-water-SPIO phantom. *J Magn Reson Imaging* 2009; **30**: 1215–22. doi: https://doi.org/10.1002/jmri.21957

26. Horng DE, Hernando D, Hines CD, Reeder SB. Comparison of R2* correction methods for accurate fat quantification in fatty liver. *J Magn Reson Imaging* 2013; **37**: 414–22. doi: https://doi.org/10.1002/jmri.23835

27. An L, Xiang QS. Chemical shift imaging with spectrum modeling. *Magn Reson Med* 2001; **46**: 126–30. doi: https://doi.org/10.1002/mrm.1167

28. Reeder SB, Wen Z, Yu H, Pineda AR, Gold GE, Markl M, et al. Multicoil Dixon chemical species separation with an iterative least-squares estimation method. *Magn Reson Med* 2004; **51**: 35–45. doi: https://doi.org/10.1002/mrm.10675

29. Reeder SB, Pineda AR, Wen Z, Shimakawa A, Yu H, Brittain JH, et al. Iterative decomposition of water and fat with echo asymmetry and least-squares estimation (IDEAL): application with fast spin-echo imaging. *Magn Reson Med* 2005; **54**: 636–44. doi: https://doi.org/10.1002/mrm.20624

30. Takasu M, Tani C, Sakoda Y, Ishikawa M, Tanitame K, Date S, et al. Iterative decomposition of water and fat with echo asymmetry and least-squares estimation (IDEAL) imaging of multiple myeloma: initial clinical efficiency results. *Eur Radiol* 2012; **22**: 1114–21. doi: https://doi.org/10.1007/s00330-011-2351-8

31. Janiczek RL, Gambarota G, Sinclair CD, Yousry TA, Thornton JS, Golay X, et al. Simultaneous T2 and lipid quantitation using IDEAL-CPMG. *Magn Reson Med* 2011; **66**: 1293–302. doi: https://doi.org/10.1002/mrm.22916

32. Fuller S, Reeder S, Shimakawa A, Yu H, Johnson J, Beaulieu C, et al. Iterative decomposition of water and fat with echo asymmetry and least-squares estimation (IDEAL) fast spin-echo imaging of the ankle: initial clinical experience. *AJR Am J Roentgenol* 2006; **187**: 1442–7. doi: https://doi.org/10.2214/AJR.05.0930

33. Reeder SB, Robson PM, Yu H, Shimakawa A, Hines CD, McKenzie CA, et al. Quantification of hepatic steatosis with MRI: the effects of accurate fat spectral modeling. *J Magn Reson Imaging* 2009; **29**: 1332–9. doi: https://doi.org/10.1002/jmri.21751

34. Yu H, Reeder SB, Shimakawa A, Brittain JH, Pelc NJ. Field map estimation with a region growing scheme for iterative 3-point water-fat decomposition. *Magn Reson Med* 2005; **54**: 1032–9. doi: https://doi.org/10.1002/mrm.20654

35. Hernando D, Kellman P, Haldar JP, Liang ZP. Robust water/fat separation in the presence of large field inhomogeneities using a graph cut algorithm. *Magn Reson Med* 2010; **63**: 79–90. doi: https://doi.org/10.1002/mrm.22177

36. Dieckmeyer M, Ruschke S, Cordes C, Yap SP, Kooijman H, Hauner H, et al. The need for T2 correction on MRS-based vertebral bone marrow fat quantification: implications for bone marrow fat fraction age dependence. *NMR Biomed* 2015; **28**: 432–9. doi: https://doi.org/10.1002/nbm.3267

37. Sullivan DC, Obuchowski NA, Kessler LG, Raunig DL, Gatsonis C, Huang EP, et al. Metrology standards for quantitative imaging biomarkers. *Radiology* 2015; **277**: 813–25. doi: https://doi.org/10.1148/radiol.2015142202

38. Bernard CP, Liney GP, Manton DJ, Turnbull LW, Langton CM. Comparison of fat quantification methods: a phantom study at 3.0T. *J Magn Reson Imaging* 2008; **27**: 192–7. doi: https://doi.org/10.1002/jmri.21201

39. Hernando D, Sharma SD, Aliyari Ghasabeh M, Alvis BD, Arora SS, Hamilton G, et al. Multisite, multivendor validation of the accuracy and reproducibility of proton-density fat-fraction quantification at 1.5T and 3T using a fat-water phantom. *Magn Reson Med* 2017; **77**: 1516–24. doi: https://doi.org/10.1002/mrm.26228

40. Bydder M, Yokoo T, Hamilton G, Middleton MS, Chavez AD, Schwimmer JB, et al. Relaxation effects in the quantification of fat using gradient echo imaging. *Magn Reson Imaging* 2008; **26**: 347–59. doi: https://doi.org/10.1016/j.mri.2007.08.012

41. Koppal S, Warntjes M, Swann J, Dyverfeldt P, Kihlberg J, Moreno R, et al. Quantitative fat and R2* mapping in vivo to measure lipid-rich necrotic core and intraplaque hemorrhage in carotid atherosclerosis. *Magn Reson Med* 2017; **78**: 285–96. doi: https://doi.org/10.1002/mrm.26359

42. Pineda AR, Reeder SB, Wen Z, Pelc NJ. Cramér-Rao bounds for three-point decomposition of water and fat. *Magn Reson Med* 2005; **54**: 625–35. doi: https://doi.org/10.1002/mrm.20623

43. Reeder SB, Sirlin CB. Quantification of liver fat with magnetic resonance imaging. *Magn Reson Imaging Clin N Am* 2010; **18**: 337–57. doi: https://doi.org/10.1016/j.mric.2010.08.013

44. Mashhood A, Railkar R, Yokoo T, Levin Y, Clark L, Fox-Bosetti S, et al. Reproducibility of hepatic fat fraction measurement by magnetic resonance imaging. *J Magn Reson Imaging* 2013; **37**: 1359–70. doi: https://doi.org/10.1002/jmri.23928

45. Latifoltojar A, Hall-Craggs M, Rabin N, Popat R, Bainbridge A, Dikaios N, et al. Whole body magnetic resonance imaging in newly diagnosed multiple myeloma: early changes in lesional signal fat fraction predict disease response. *Br J Haematol* 2017; **176**: 222–33. doi: https://doi.org/10.1111/bjh.14401

46. Alberti KG, Eckel RH, Grundy SM, Zimmet PZ, Cleeman JI, Donato KA, et al. Harmonizing the metabolic syndrome: a joint interim statement of the International Diabetes Federation Task Force on Epidemiology and Prevention; National Heart, Lung, and Blood Institute; American Heart Association; World Heart Federation; International Atherosclerosis Society; and International Association for the Study of Obesity. *Circulation* 2009; **120**: 1640–5. doi: https://doi.org/10.1161/CIRCULATIONAHA.109.192644

47. Arulanandan A, Ang B, Bettencourt R, Hooker J, Behling C, Lin GY, et al. Association between quantity of liver fat and cardiovascular risk in patients with nonalcoholic fatty liver disease independent of nonalcoholic steatohepatitis. *Clin Gastroenterol Hepatol* 2015; **13**: 1513–20. doi: https://doi.org/10.1016/j.cgh.2015.01.027

48. Marchesini G, Bugianesi E, Forlani G, Cerrelli F, Lenzi M, Manini R, et al. Nonalcoholic fatty liver, steatohepatitis, and the metabolic syndrome. *Hepatology* 2003; **37**: 917–23. doi: https://doi.org/10.1053/jhep.2003.50161

49. Powell EE, Jonsson JR, Clouston AD. Dangerous liaisons: the metabolic syndrome and nonalcoholic fatty liver disease. *Ann Intern Med* 2005; **143**: 753. doi: https://doi.org/10.7326/0003-4819-143-10-200511150-00015

50. Clark JM, Diehl AM. Defining nonalcoholic fatty liver disease: implications for epidemiologic studies. *Gastroenterology* 2003; **124**: 248–50. doi: https://doi.org/10.1053/gast.2003.50032

51. Grundy SM. Hypertriglyceridemia, insulin resistance, and the metabolic syndrome. *Am J Cardiol* 1999; **83**: 25–9. doi: https://doi.org/10.1016/S0002-9149(99)00211-8

52. Sanyal AJ. Mechanisms of Disease: pathogenesis of nonalcoholic fatty liver disease. *Nat Clin Pract Gastroenterol Hepatol* 2005; **2**: 46–53. doi: https://doi.org/10.1038/ncpgasthep0084

53. Tiniakos DG, Vos MB, Brunt EM. Nonalcoholic fatty liver disease: pathology and pathogenesis. *Annu Rev Pathol* 2010; **5**: 145–71. doi: https://doi.org/10.1146/annurev-pathol-121808-102132

54. Day CP, James OF. Steatohepatitis: a tale of two "hits"? *Gastroenterology* 1998; **114**: 842–5. doi: https://doi.org/10.1016/S0016-5085(98)70599-2

55. Schuppan D, Schattenberg JM. Non-alcoholic steatohepatitis: pathogenesis and novel therapeutic approaches. *J Gastroenterol Hepatol* 2013; **28**(Supp 1): 68–76. doi: https://doi.org/10.1111/jgh.12212

56. European Association for the Study of the Liver (EASL), European Association for the Study of Diabetes (EASD), European Association for the Study of Obesity (EASO). EASL-EASD-EASO clinical practice guidelines for the management of non-alcoholic fatty liver disease. *J Hepatol* 2016; **64**: 1388–402. doi: https://doi.org/10.1016/j.jhep.2015.11.004

57. Chalasani N, Younossi Z, Lavine JE, Diehl AM, Brunt EM, Cusi K, et al. The diagnosis and management of non-alcoholic fatty liver disease: practice guideline by the American Association for the Study of Liver Diseases, American College of Gastroenterology, and the American Gastroenterological Association. *Hepatology* 2012; **55**: 2005–23. doi: https://doi.org/10.1002/hep.25762

58. Vilgrain V, Ronot M, Abdel-Rehim M, Zappa M, d'Assignies G, Bruno O, et al. Hepatic steatosis: a major trap in liver imaging. *Diagn Interv Imaging* 2013; **94**: 713–27. doi: https://doi.org/10.1016/j.diii.2013.03.010

59. Heba ER, Desai A, Zand KA, Hamilton G, Wolfson T, Schlein AN, et al. Accuracy and the effect of possible subject-based confounders of magnitude-based MRI for estimating hepatic proton density fat fraction in adults, using MR spectroscopy as reference. *J Magn Reson Imaging* 2016; **43**: 398–406. doi: https://doi.org/10.1002/jmri.25006

60. Idilman IS, Tuzun A, Savas B, Elhan AH, Celik A, Idilman R, et al. Quantification of liver, pancreas, kidney, and vertebral body MRI-PDFF in non-alcoholic fatty liver disease. *Abdom Imaging* 2015; **40**: 1512–9. doi: https://doi.org/10.1007/s00261-015-0385-0

61. Imajo K, Kessoku T, Honda Y, Tomeno W, Ogawa Y, Mawatari H, et al. Magnetic resonance imaging more accurately classifies steatosis and fibrosis in patients with nonalcoholic fatty liver disease than transient elastography. *Gastroenterology* 2016; **150**: 626–37. doi: https://doi.org/10.1053/j.gastro.2015.11.048

62. Park CC, Nguyen P, Hernandez C, Bettencourt R, Ramirez K, Fortney L, et al. Magnetic resonance elastography vs transient elastography in detection of fibrosis and noninvasive measurement of steatosis in patients with biopsy-proven nonalcoholic fatty liver disease. *Gastroenterology* 2017; **152**: 598–607. doi: https://doi.org/10.1053/j.gastro.2016.10.026

63. Bannas P, Kramer H, Hernando D, Agni R, Cunningham AM, Mandal R, et al. Quantitative magnetic resonance imaging of hepatic steatosis: validation in ex vivo human livers. *Hepatology* 2015; **62**: 1444–55. doi: https://doi.org/10.1002/hep.28012

64. Paparo F, Cenderello G, Revelli M, Bacigalupo L, Rutigliani M, Zefiro D, et al. Diagnostic value of MRI proton density fat fraction for assessing liver steatosis in chronic viral C hepatitis. *Biomed Res Int* 2015; **2015**: 1–11. doi: https://doi.org/10.1155/2015/758164

65. Runge JH, Bakker PJ, Gaemers IC, Verheij J, Hakvoort TB, Ottenhoff R, et al. Measuring liver triglyceride content in mice: non-invasive magnetic resonance methods as an alternative to histopathology. *MAGMA* 2014; **27**: 317–27. doi: https://doi.org/10.1007/s10334-013-0414-3

66. Yokoo T, Pirasteh A, Bashir M, Tang A, Kukuk GM, Kuhn J. Proton-density fat fraction biomarker committee: A meta-analysis interim report 2016. *J Magn Reson Imaging* 2016; **36**: 1011–4.

67. Schwimmer JB, Middleton MS, Behling C, Newton KP, Awai HI, Paiz MN, et al. Magnetic resonance imaging and liver histology as biomarkers of hepatic steatosis in children with nonalcoholic fatty liver disease. *Hepatology* 2015; **61**: 1887–95. doi: https://doi.org/10.1002/hep.27666

68. Tang A, Tan J, Sun M, Hamilton G, Bydder M, Wolfson T, et al. Nonalcoholic fatty liver disease: MR imaging of liver proton density fat fraction to assess hepatic steatosis. *Radiology* 2013; **267**: 422–31. doi: https://doi.org/10.1148/radiol.12120896

69. Le TAT, Chen J, Changchien C, Peterson MR, Cohen BL, Kono Y. Effect of colesevelam on magnetic resonance imaging derived fat maps in nonalcoholic steatohepatitis: a randomized controlled trial. *Gastroenterology* 2012; **142**: S-1014–32. doi: https://doi.org/10.1016/S0016-5085(12)63926-2

70. Noureddin M, Lam J, Peterson MR, Middleton M, Hamilton G, Le TA, et al. Utility of magnetic resonance imaging versus histology for quantifying changes in liver fat in nonalcoholic fatty liver disease trials. *Hepatology* 2013; **58**: 1930–40. doi: https://doi.org/10.1002/hep.26455

71. Tang A, Rabasa-Lhoret R, Castel H, Wartelle-Bladou C, Gilbert G, Massicotte-Tisluck K, et al. Effects of insulin glargine and liraglutide therapy on liver fat as measured by magnetic resonance in patients with type 2 diabetes: randomized trial. *Diabetes Care* 2015; **38**: 1339–46. doi: https://doi.org/10.2337/dc14-2548

72. Bonekamp S, Tang A, Mashhood A, Wolfson T, Changchien C, Middleton MS, et al. Spatial distribution of MRI-determined hepaticprotondensityfatfraction in adults with nonalcoholicfattyliverdisease. *J Magn Reson Imaging* 2014; **39**: 1525–32. doi: https://doi.org/10.1002/jmri.24321

73. Kim KY, Song JS, Kannengiesser S, Han YM. Hepatic fat quantification using the proton density fat fraction (PDFF): utility of free-drawn-PDFF with a large coverage area. *Radiol Med* 2015; **120**: 1083–93. doi: https://doi.org/10.1007/s11547-015-0545-x

74. VuKN, Gilbert G, Chalut M, Chagnon M, Chartrand G, Tang A. MRI-determined liver proton density fat fraction, with MRS validation: Comparison of regions of interest sampling methods in patients with type 2 diabetes. *J Magn Reson Imaging* 2016; **43**: 1090–9. doi: https://doi.org/10.1002/jmri.25083

75. Chouhan MD, Ambler G, Mookerjee RP, Taylor SA. Multiparametric magnetic resonance imaging to predict clinical outcomes in patients with chronic liver disease: a cautionary note on a promising technique. *J Hepatol* 2017; **66**: 455–7. doi: https://doi.org/10.1016/j.jhep.2016.09.026

76. Smits MM, van Geenen EJ. The clinical significance of pancreatic steatosis. *Nat Rev Gastroenterol Hepatol* 2011; **8**: 169–77. doi: https://doi.org/10.1038/nrgastro.2011.4

77. Mathur A, Marine M, Lu D, Swartz-Basile DA, Saxena R, Zyromski NJ, et al. Nonalcoholic fatty pancreas disease. *HPB* 2007; **9**: 312–8. doi: https://doi.org/10.1080/13651820701504157

78. Tariq H, Nayudu S, Akella S, Glandt M. Chilimuri SN-AFPDAR of L. Non-alcoholic fatty pancreatic disease: a review of literature. *Gastroenterol Res* 2016; **9**: 87–91.

79. Lee Y, Lingvay I, Szczepaniak LS, Ravazzola M, Orci L, Unger RH. Pancreatic steatosis: harbinger of type 2 diabetes in obese rodents. *Int J Obes* 2010; **34**: 396–400. doi: https://doi.org/10.1038/ijo.2009.245

80. Singh RG, Yoon HD, Wu LM, Lu J, Plank LD, Petrov MS. Ectopic fat accumulation in the pancreas and its clinical relevance: a systematic review, meta-analysis, and meta-regression. *Metabolism* 2017; **69**: 1–13. doi: https://doi.org/10.1016/j.metabol.2016.12.012

81. Ou HY, Wang CY, Yang YC, Chen MF, Chang CJ. The association between nonalcoholic fatty pancreas disease and diabetes. *PLoS One* 2013; **8**: e62561. doi: https://doi.org/10.1371/journal.pone.0062561

82. Saisho Y, Butler AE, Meier JJ, Monchamp T, Allen-Auerbach M, Rizza RA, et al. Pancreas volumes in humans from birth to age one hundred taking into account sex, obesity, and presence of type-2 diabetes. *Clin Anat* 2007; **20**: 933–42. doi: https://doi.org/10.1002/ca.20543

83. Tushuizen ME, Bunck MC, Pouwels PJ, Bontemps S, van Waesberghe JH, Schindhelm RK, et al. Pancreatic fat content and beta-cell function in men with and without type 2 diabetes. *Diabetes Care* 2007; **30**: 2916–21. doi: https://doi.org/10.2337/dc07-0326

84. Wong VW, Wong GL, Yeung DK, Abrigo JM, Kong AP, Chan RS, et al. Fatty pancreas, insulinresistance, and β-cellfunction: apopulationstudyusingfat-watermagneticresonanceimaging. *Am J Gastroenterol* 2014; **109**: 589–97. doi: https://doi.org/10.1038/ajg.2014.1

85. Staaf J, Labmayr V, Paulmichl K, Manell H, Cen J, Ciba I, et al. Pancreatic fat is associated with metabolic syndrome and visceral fat but not beta-cell function or body mass index in pediatric obesity. *Pancreas* 2017; **46**: 358–65. doi: https://doi.org/10.1097/MPA.0000000000000771

86. Patel NS, Peterson MR, Brenner DA, Heba E, Sirlin C, Loomba R. Association between novel MRI-estimated pancreatic fat and liver histology-determined steatosis and fibrosis in non-alcoholic fatty liver disease. *Aliment Pharmacol Ther* 2013; **37**: 630–9. doi: https://doi.org/10.1111/apt.12237

87. Patel NS, Peterson MR, Lin GY, Feldstein A, Schnabl B, Bettencourt R, et al. Insulin resistance increases MRI-estimated pancreatic fat in nonalcoholic fatty liver disease and normal controls. *Gastroenterol Res Pract* 2013; **2013**: 1–8. doi: https://doi.org/10.1155/2013/498296

88. Yoon JH, Lee JM, Lee KB, Kim SW, Kang MJ, Jang JY, et al. Pancreatic steatosis and fibrosis: quantitative assessment with preoperative multiparametric MR imaging. *Radiology* 2016; **279**: 140–50. doi: https://doi.org/10.1148/radiol.2015142254

89. Henninger B, Rauch S, Zoller H, Plaikner M, Jaschke W, Kremser C. R2*-relaxometry of the pancreas in patients with human hemochromatosis protein associated hereditary hemochromatosis. *Eur J Radiol* 2017; **89**: 149–55. doi: https://doi.org/10.1016/j.ejrad.2017.02.006

90. Pfeifer CD, Schoennagel BP, Grosse R, Wang ZJ, Graessner J, Nielsen P, et al. Pancreatic iron and fat assessment by MRI-R2* in patients with iron overload diseases. *J Magn Reson Imaging* 2015; **42**: 196–203. doi: https://doi.org/10.1002/jmri.24752

91. Rosen CJ, Bouxsein ML. Mechanisms of disease: is osteoporosis the obesity of bone? *Nat Clin Pract Rheumatol* 2006; **2**: 35–43. doi: https://doi.org/10.1038/ncprheum0070

92. Wren TA, Chung SA, Dorey FJ, Bluml S, Adams GB, Gilsanz V. Bone marrow fat is inversely related to cortical bone in young and old subjects. *J Clin Endocrinol Metab* 2011; **96**: 782–6. doi: https://doi.org/10.1210/jc.2010-1922

93. Shen W, Chen J, Gantz M, Punyanitya M, Heymsfield SB, Gallagher D, et al. MRI-measured pelvic bone marrow adipose tissue is inversely related to DXA-measured bone mineral in younger and older adults. *Eur J Clin Nutr* 2012; **66**: 983–8. doi: https://doi.org/10.1038/ejcn.2012.35

94. Cohen A, Dempster DW, Stein EM, Nickolas TL, Zhou H, McMahon DJ, et al. Increased marrow adiposity in premenopausal women with idiopathic osteoporosis. *J Clin Endocrinol Metab* 2012; **97**: 2782–91. doi: https://doi.org/10.1210/jc.2012-1477

95. Griffith JF, Yeung DK, Antonio GE, LeeFK, Hong AW, Wong SY, et al. Vertebral bone mineral density, marrow perfusion, and fat content in healthy men and men with osteoporosis: dynamic contrast-enhanced MR imaging and MR spectroscopy. *Radiology* 2005; **236**: 945–51. doi: https://doi.org/10.1148/radiol.2363041425

96. Wronski TJ, Smith JM, Jee WS. Variations in mineral apposition rate of trabecular bone within the beagle skeleton. *Calcif Tissue Int* 1981; **33**: 583–6. doi: https://doi.org/10.1007/BF02409495

97. Li M, Shen Y, Qi H, Wronski TJ. Comparative study of skeletal response to estrogen depletion at red and yellow marrow sites in rats. *Anat Rec* 1996; **245**: 472–80. doi: https://doi.org/10.1002/(SICI)1097-0185(199607)245:3<472::AID-AR3>3.0.CO;2-U

98. Takeda S, Elefteriou F, Levasseur R, Liu X, Zhao L, Parker KL, et al. Leptin regulates bone formation via the sympathetic nervous system. *Cell* 2002; **111**: 305–17. doi: https://doi.org/10.1016/S0092-8674(02)01049-8

99. Ducy P, Amling M, Takeda S, Priemel M, Schilling AF, Beil FT, et al. Leptin inhibits bone formation through a hypothalamic relay: a central control of bone mass. *Cell* 2000; **100**: 197–207.

100. LiGW, Xu Z, Chen QW, Chang SX, Tian YN, Fan JZ. The temporal characterization of marrow lipids and adipocytes in a rabbit model of glucocorticoid-induced osteoporosis. *Skeletal Radiol* 2013; **42**: 1235–44. doi: https://doi.org/10.1007/s00256-013-1659-7

101. Tornvig L, Mosekilde LI, Justesen J, Falk E, Kassem M. Troglitazone treatment increases bone marrow adipose tissue volume but does not affect trabecular bone volume in mice. *Calcif Tissue Int* 2001; **69**: 46–50. doi: https://doi.org/10.1007/s002230020018

102. Bredella MA, Lin E, Gerweck AV, Landa MG, Thomas BJ, Torriani M, et al. Determinants of bone microarchitecture and mechanical properties in obese men. *J Clin Endocrinol Metab* 2012; **97**: 4115–22. doi: https://doi.org/10.1210/jc.2012-2246

103. Bredella MA, Torriani M, Ghomi RH, Thomas BJ, Brick DJ, Gerweck AV, et al. Vertebral bone marrow fat is positively associated with visceral fat and inversely associated with IGF-1 in obese women. *Obesity* 2011; **19**: 49–53. doi: https://doi.org/10.1038/oby.2010.106

104. Rosen CJ, Ackert-Bicknell CL, Adamo ML, Shultz KL, Rubin J, Donahue LR, et al. Congenic mice with

low serum IGF-I have increased body fat, reduced bone mineral density, and an altered osteoblast differentiation program. *Bone* 2004; **35**: 1046–58. doi: https://doi.org/10.1016/j.bone.2004.07.008

105. Russo GT, Giandalia A, Romeo EL, Nunziata M, Muscianisi M, Ruffo MC, et al. Fracture risk in type 2 diabetes: current perspectives and gender differences. *Int J Endocrinol* 2016; **2016**: 1–11. doi: https://doi.org/10.1155/2016/1615735

106. Wongdee K, Charoenphandhu N. Update on type 2 diabetes-related osteoporosis. *World J Diabetes* 2015; **6**: 673–8. doi: https://doi.org/10.4239/wjd.v6.i5.673

107. Patsch JM, Li X, Baum T, Yap SP, Karampinos DC, Schwartz AV, et al. Bone marrow fat composition as a novel imaging biomarker in postmenopausal women with prevalent fragility fractures. *J Bone Miner Res* 2013; **28**: 1721–8. doi: https://doi.org/10.1002/jbmr.1950

108. Baum T, Yap SP, Karampinos DC, Nardo L, Kuo D, Burghardt AJ, et al. Does vertebral bone marrow fat content correlate with abdominal adipose tissue, lumbar spine bone mineral density, and blood biomarkers in women with type 2 diabetes mellitus? *J Magn Reson Imaging* 2012; **35**: 117–24. doi: https://doi.org/10.1002/jmri.22757

109. Yeung DK, Griffith JF, Antonio GE, Lee FK, Woo J, Leung PC. Osteoporosis is associated with increased marrow fat content and decreased marrow fat unsaturation: a proton MR spectroscopy study. *J Magn Reson Imaging* 2005; **22**: 279–85. doi: https://doi.org/10.1002/jmri.20367

110. Devlin MJ, Cloutier AM, Thomas NA, Panus DA, Lotinun S, Pinz I, et al. Caloric restriction leads to high marrow adiposity and low bone mass in growing mice. *J Bone Miner Res* 2010; **25**: 2078–88. doi: https://doi.org/10.1002/jbmr.82

111. Bredella MA, Fazeli PK, Miller KK, Misra M, Torriani M, Thomas BJ, et al. Increased bone marrow fat in anorexia nervosa. *J Clin Endocrinol Metab* 2009; **94**: 2129–36. doi: https://doi.org/10.1210/jc.2008-2532

112. Rajkumar SV, Dimopoulos MA, Palumbo A, Blade J, Merlini G, Mateos MV, et al. International yyeloma working group updated criteria for the diagnosis of multiple myeloma. *Lancet Oncol* 2014; **15**: e538–48e548. doi: https://doi.org/10.1016/S1470-2045(14)70442-5

113. Excellence NI of H and C. *Myeloma: diagnosis and management NG35*. London, UK: NICE; 2016.

114. Takasu M, Kaichi Y, Tani C, Date S, Akiyama Y, Kuroda Y, et al. Iterative decomposition of water and fat with echo asymmetry and least-squares estimation (IDEAL) magnetic resonance imaging as a biomarker for symptomatic multiple myeloma. *PLoS One* 2015; **10**: : e0116842: . doi: https://doi.org/10.1371/journal.pone.0116842

115. Costelloe CM, Kundra V, Ma J, Chasen BA, Rohren EM, Bassett RL, et al. Fast Dixon whole-body MRI for detecting distant cancer metastasis: a preliminary clinical study. *J Magn Reson Imaging* 2012; **35**: 399–408. doi: https://doi.org/10.1002/jmri.22815

116. Lee SH, Lee YH, Hahn S, Suh JS. Fat fraction estimation of morphologically normal lumbar vertebrae using the two-point mDixon turbo spin-echo MRI with flexible echo times and multipeak spectral model of fat: Comparison between cancer and non-cancer patients. *Magn Reson Imaging* 2016; **34**: 1114–20. doi: https://doi.org/10.1016/j.mri.2016.05.007

117. Sieper J, Rudwaleit M, Baraliakos X, Brandt J, Braun J, Burgos-Vargas R, et al. The Assessment of Spondylo Arthritis international Society (ASAS) handbook: a guide to assess spondyloarthritis. *Ann Rheum Dis* 2009; **68**(Suppl 2): ii1–ii44. doi: https://doi.org/10.1136/ard.2008.104018

118. Maksymowych WP, Inman RD, Salonen D, Dhillon SS, Williams M, Stone M, et al. Spondyloarthritis research consortium of Canada magnetic resonance imaging index for assessment of sacroiliac joint inflammation in ankylosing spondylitis. *Arthritis Rheum* 2005; **53**: 703–9. doi: https://doi.org/10.1002/art.21445

119. Arnbak B, Jensen TS, Manniche C, Zejden A, Egund N, Jurik AG. Spondyloarthritis-related and degenerative MRI changes in the axial skeleton - an inter- and intra-observer agreement study. *BMC Musculoskelet Disord* 2013; **14**: 274. doi: https://doi.org/10.1186/1471-2474-14-274

120. Bray TJP, Bainbridge A, Punwani S, Ioannou Y, Hall-Craggs MA. Simultaneous Quantification of Bone Edema/Adiposity and Structure in Inflamed Bone Using Chemical Shift-Encoded MRI in Spondyloarthritis. *Magn Reson Med* 2017; [Epub ahead of print]. doi: https://doi.org/10.1002/mrm.26729

121. Latifoltojar A, Hall-Craggs M, Bainbridge A, Rabin N, Popat R, Rismani A, et al. Whole-body MRI quantitative biomarkers are associated significantly with treatment response in patients with newly diagnosed symptomatic multiple myeloma following bortezomib induction. *Eur Radiol* 2017; (Epub of head of print). doi: https://doi.org/10.1007/s00330-017-4907-8

122. Morrow JM, Sinclair CD, Fischmann A, Machado PM, Reilly MM, Yousry TA, et al. MRI biomarker assessment of neuromuscular disease progression: a prospective observational cohort study. *Lancet Neurol* 2016; **15**: 65–77. doi: https://doi.org/10.1016/S1474-4422(15)00242-2

123. Yao L, Yip AL, Shrader JA, Mesdaghinia S, Volochayev R, Jansen AV, et al. Magnetic resonance measurement of muscle T2, fat-corrected T2 and fat fraction in the assessment of idiopathic inflammatory myopathies. *Rheumatology* 2016; **55**: 441–9. doi: https://doi.org/10.1093/rheumatology/kev344

124. Hiba B, Richard N, Hébert LJ, Coté C, Nejjari M, Vial C, et al. Quantitative assessment of skeletal muscle degeneration in patients with myotonic dystrophy type 1 using MRI. *J Magn Reson Imaging* 2012; **35**: 678–85. doi: https://doi.org/10.1002/jmri.22849

125. Gaeta M, Scribano E, Mileto A, Mazziotti S, Rodolico C, Toscano A, et al. Muscle fat fraction in neuromuscular disorders: dual-echo dual-flip-angle spoiled gradient-recalled MR imaging technique for quantification-a feasibility study. *Radiology* 2011; **259**: 487–94. doi: https://doi.org/10.1148/radiol.10101108

126. Kellman P, Hernando D, Arai AE. Myocardial fat imaging. *Curr Cardiovasc Imaging Rep* 2010; **3**: 83–91. doi: https://doi.org/10.1007/s12410-010-9012-1

127. Arnold JR, Karamitsos TD, Pegg TJ, Francis JM, Neubauer S. Left ventricular lipomatous metaplasia following myocardial infarction. *Int J Cardiol* 2009; **137**: e11–e12. doi: https://doi.org/10.1016/j.ijcard.2008.05.039

128. Wu YW, Tadamura E, Yamamuro M, Kanao S, Abe M, Kimura T, et al. Identification of lipomatous metaplasia in old infarcted myocardium by cardiovascular magnetic resonance and computed tomography. *Int J Cardiol* 2007; **115**: E15–E16. doi: https://doi.org/10.1016/j.ijcard.2006.07.094

129. Baroldi G, Silver MD, De Maria R, Parodi O, Pellegrini A. Lipomatous metaplasia in left ventricular scar. *Can J Cardiol* 1997; **13**: 65–71.

130. Lu M, Zhao S, Jiang S, Yin G, Wang C, Zhang Y, et al. Fat deposition in dilated cardiomyopathy assessed by CMR. *JACC Cardiovasc Imaging* 2013; **6**: 889–98. doi: https://doi.org/10.1016/j.jcmg.2013.04.010

131. Goldfarb JW, Roth M, Han J. Myocardial fat deposition after left ventricular myocardial infarction: assessment by using MR water-fat separation imaging. *Radiology* 2009; **253**: 65–73. doi: https://doi.org/10.1148/radiol.2532082290

132. Farrelly C, Shah S, Davarpanah A, Keeling AN, Carr JC. ECG-gated multiecho Dixon fat-water separation in cardiac MRI: advantages over conventional fat-saturated imaging. *AJR Am J Roentgenol* 2012; **199**: W74–W83. doi: https://doi.org/10.2214/AJR.11.7759

133. Liu CY, Redheuil A, Ouwerkerk R, Lima JA, Bluemke DA. Myocardial fat quantification in humans: evaluation by two-point water-fat imaging and localized proton spectroscopy. *Magn Reson Med* 2010; **63**: 892–901. doi: https://doi.org/10.1002/mrm.22289